HHS Public Access

Author manuscript

Curr Protoc Mouse Biol. Author manuscript; available in PMC 2017 March 01.

Published in final edited form as:

Curr Protoc Mouse Biol. ; 6(1): 15–38. doi:10.1002/9780470942390.mo150122.

Cardiovascular Imaging in Mice

Colin K.L. Phoon[1] and **Daniel H. Turnbull**[2,3]

[1]Division of Pediatric Cardiology, Department of Pediatrics, New York University School of Medicine, New York, New York

[2]Departments of Radiology and Pathology, New York University School of Medicine, New York, New York

[3]Skirball Institute of Biomolecular Medicine, New York University School of Medicine, New York, New York

Abstract

The mouse is the mammalian model of choice for investigating cardiovascular biology, given our ability to manipulate it by genetic, pharmacologic, mechanical, and environmental means. Imaging is an important approach to phenotyping both function and structure of cardiac and vascular components. This review details commonly used imaging approaches, with a focus on echocardiography and magnetic resonance imaging and brief overviews of other imaging modalities. We also briefly outline emerging imaging approaches but caution that reliability and validity data may be lacking.

Keywords

Doppler; echocardiography; magnetic resonance imaging; mouse models; ultrasound biomicroscopy

INTRODUCTION

Cardiovascular diseases remain a leading cause of morbidity and mortality around the world, but particularly in developed societies (Mozaffarian et al., 2015). Much of the research into their causes and treatments relies on animal models. The mouse has emerged as the mammalian model of choice, due to its parallels to human cardiovascular physiology and human development, as well as our ability to modify mouse genetics. Cardiovascular imaging plays an important role in studying adult mouse cardiovascular physiology and pathophysiological processes, where important questions focus on myocardial infarction, atherosclerosis, pathologic hypertrophy, and heart failure. In addition, investigations into cardiovascular development are important for several reasons. First, congenital heart defects are the most common birth defect, occurring in approximately 1% of all live births; prenatal incidence is approximately 10-fold higher than postnatal incidence (Hoffman, 1995; Hoffman and Kaplan, 2002). Second, the concerted effort that is the International Mouse

CONFLICTS OF INTEREST

Drs. Phoon and Turnbull have no conflicts of interest to disclose.

Phenotyping Consortium aims to knock out every single gene in the mouse genome, and it is estimated this will lead to prenatal lethality in some 30% of knockouts; thus, there will be a wealth of information on how gene function affects embryonic development and how loss of many genes will affect cardiovascular processes (Adams et al., 2013; Norris et al., 2013). Finally, an understanding of heart development and particularly myocardial development forms the basis for much of regenerative cardiovascular medicine.

Imaging of mouse cardiovascular biology focuses primarily on myocardial and vascular function. Cardiac and vascular imaging in mice is challenging due to the small size of these structures, high heart rates, and the need, in most cases, for sedation. Most in vivo cardiovascular imaging is accomplished using ultrasound (echocardiography; high-resolution ultrasound is also called ultrasound biomicroscopy [UBM]) and to a lesser extent, magnetic resonance imaging (MRI). Imaging systems must be optimized for adequate spatial and temporal resolution, all the while maintaining as close to normal a physiological state as possible. Trade-offs in structural visualization and high frame rates, however, may be acceptable depending on the question being addressed. For most mouse biologists, echocardiography is readily available, although local expertise in hands-on imaging may be variable; therefore, this review focuses in more detail on cardiovascular ultrasound imaging. MRI is a more specialized approach and complements cardiovascular ultrasound in specific circumstances. In this article, we detail experimental imaging protocols commonly used in our laboratories in both the prenatal and postnatal mouse, while also touching on additional imaging options in more specialized areas.

IMAGING CONSCIOUS VERSUS ANESTHETIZED MICE: CONSIDERATIONS FOR ANESTHESIA

Concerns about anesthesia include depression of myocardial function and heart rate, as well as autonomic reflex control. Echocardiography can be performed in either conscious or anesthetized mice. (Note: MRI cannot be done in conscious mice.) While some investigators have advocated for echocardiography of conscious mice due to a more physiological state, this approach requires training the mice over several days prior to imaging—which may not be feasible for studies of cardiovascular development—and can also result in stress in the mouse during imaging, resulting in physiological variability. Different anesthetics exhibit different effects on cardiovascular physiology; none are perfect. A recent study from the Vatner lab suggests that intraperitoneal avertin alone may exert the least effects on cardiovascular parameters (Pachon et al., 2015). Moreover, at least one study has suggested that deep sedation with morphine/midazolam exerted less of a depressive effect on cardiac function than general anesthesia with isoflurane in mice undergoing MRI imaging (Berry et al., 2009). Ketamine/xylazine fared worse than isoflurane, however (Kober et al., 2004), and it should be noted that one needs to consider the respiratory artifacts induced by different concentrations of isoflurane (Kober et al., 2004). Most labs use inhalational isoflurane, which had been touted by Roth et al. (2002) as the optimal anesthetic agent. Our labs use primarily isoflurane; importantly, we use a consistent approach to anesthesia for all mice, to reduce variability between mice and experimental groups. We also believe isoflurane is the preferred anesthetic when serial (e.g., daily) imaging is required—as we have performed in

certain experimental protocols (Phoon et al., 2007; Nomura-Kitabayashi et al., 2009)—as we have concerns about the pharmacokinetics and half-lives of injectable anesthetics when administered daily. Detailed data on effects of anesthesia are beyond the scope of this article and can be found elsewhere (Roth et al., 2002; Gao et al., 2011; Pachon et al., 2015).

CARDIAC IMAGING: ULTRASOUND (ECHOCARDIOGRAPHY)

Postnatal Echocardiography: Neonatal, Juvenile, and Adult

Mouse cardiac imaging (echocardiography) has been in use for ~2 decades, at first employing clinical imaging systems coupled to transducers meant for human clinical use (Manning et al., 1994; Gardin et al., 1995; Collis et al., 2007). More recently—for approximately the past 15 years—high-frequency systems have been available that permit adequate spatial resolution for true mouse cardiac work. Modern, phased array imaging systems offer not only high spatial resolution but also the temporal resolution needed for the very rapid mouse heart rates. In general, 40 MHz center frequency transducers will achieve an axial resolution of 40 to 70 μm, which is more than adequate for a left ventricle (LV) that is typically 2 to 4 mm internal diameter. The temporal resolution of current imaging systems is now in the range of 200 to 500 frames/sec, depending on the field of view. A history of the technical innovations leading to “micro-ultrasound” (ultrasound biomicroscopy) was published by Foster et al. (2011).

The goals of mouse cardiac imaging include: (1) functional analysis of the myocardium, typically of the LV; (2) functional analysis of valves, mostly the left-sided valves (mitral and aortic); (3) analysis of flow, for example in transverse aortic constriction; and (4) miscellaneous applications, including pulmonary artery flow and right ventricle analysis. Most of the literature on mouse echocardiography focuses on effects of genetic, pharmacologic, and mechanical manipulation (coronary ligation, transverse aortic constriction) of the LV, reflecting the highest-priority heart diseases of coronary artery disease, heart failure, and cardiomyopathy.

NOTE: All protocols using live animals must first be reviewed and approved by an Institutional Animal Care and Use Committee (IACUC) and must conform to governmental regulations regarding the care and use of laboratory animals.

Materials

Mouse of interest

Isoflurane

Medical oxygen (optional)

70% ethanol

Depilatory cream (if fur clippers are used for shaving)

Ultrasound (acoustic coupling) gel

Scale (to weigh mouse)

Anesthesia setup

Anesthetic induction chamber

Isoflurane distributor

Mouse anesthesia nosecone delivery system

High-resolution ultrasound imaging system coupled to the anesthesia setup and to a warming pad that doubles as an imaging platform

Electrocardiography (EKG) system including EKG leads and electrodes (usually incorporated into imaging platform)

Strips of tape, cut to size (for paws)

Hair dryer (for warm air convection) or warming lamp

Razor blade (not safety razor) or fur clippers

Gauze pads or Kimwipes

Thermistor

1. Weigh mouse.

   Mouse can be weighed after falling asleep as well.

2. Place the mouse in the anesthetic induction chamber.

3. Mix isoflurane with medical oxygen, typically 2% to 3% at 1 liter/min flow, to induce sedation in the induction chamber.

   Room air will also work in place of medical oxygen, but one must be consistent in all experiments.

   Sedation typically occurs within 1 to 2 min, when the mouse is still and breathing slowly.

4. Quickly transfer the mouse from the induction chamber to the imaging platform, and place its nose in the anesthetic nosecone. Re-route the isoflurane/oxygen mixture to the warming pad/imaging platform but maintain at the higher level until after removing fur. Determine the level of sedation by paw pinch, corneal reflex, and level of respirations (both rate and amplitude).

5. Tape the paws to the EKG leads on the warming platform.

   The tips of the paws should be uncovered so the EKG electrode gel can make contact with both the paws and the EKG pads on the platform.

   In addition to monitoring the anesthetized mouse, the EKG can detect cardiac rhythm disturbances that may lead to further scientific questions in a particular mouse model (Danielson et al., 2013).

6. Remove fur from the chest as follows:

a. Apply a generous amount of 70% ethanol to both the left chest and most of the right chest, including the superior (cranial) and inferior (caudal) margins of the thoracic cage.

Use ethanol for shaving lubricant as water does not work as well, and creams will be difficult to wipe off. However, this should not be so much as to have excessive ethanol run off onto the imaging platform and tape at the paws.

b. Use the razor blade to carefully shave the chest.

The shaved fur can be wiped off with a gauze pad or Kimwipe.

Alternatively, fur clippers can be used, followed by depilatory cream. Be careful in this instance not to leave the cream on the chest for too long, which will irritate the skin. Less than 1 min should be adequate. Once the cream is wiped off, clean the skin with a water-soaked gauze pad to remove traces of the depilatory cream.

7. Reduce the isoflurane to 1%. Determine the level of sedation by paw pinch, corneal reflex, and level of respirations (both rate and amplitude).

8. Begin warm air convection.

9. Insert the thermistor probe into the rectum.

The probe should be well in, and taped securely in place, to accurately reflect the core temperature of the mouse

10. Apply EKG gel to paws and EKG leads, and adjust the EKG tracing on the imaging system.

Acoustic coupling gel can double as EKG gel.

Many investigators call for warming the gel. In our experience, the gel cools quickly upon application to the chest anyway, so we find this unnecessary. However, this will not hurt.

11. Once the core temperature is physiological and stable (takes several minutes) with a stable heart rate (see Roth et al., 2002), apply the acoustic coupling gel to the chest.

In our experience, it will take several minutes for the core temperature to rise to the 37°C to 38°C range. Acoustic coupling gel may decrease the temperature slightly, but when applied to the mouse chest, generally does not affect this much.

Heart rates of sedated or anesthetized mice are typically 400 to 500 bpm. This will be higher for conscious mice (600 to 700 bpm), which we do not discuss in detail here.

12. Optimize the acoustic windows; make sure the fur is completely removed.

Sometimes, lung can interfere with imaging, and tilting the imaging platform to the left may help. Conversely, one should be flexible in imaging from the right parasternal windows; for unclear reasons, we find sometimes the heart is shifted rightward. Ribs and sternum may also create "ultrasound shadow" artifacts, and one may need to make minute (<mm) adjustments in transducer positioning to achieve the best imaging window.

Imaging can be done using the stand or freehand. We prefer freehand imaging, as adjustments can be made quickly, but this requires more practice and experience to obtain consistent imaging planes. If trying to obtain multiple views (parasternal long and short axes, apical views, aorta), then the freehand method is the fastest.

There appears to be little difference whether the mouse is lying supine or tilted somewhat in a decubitus position. Therefore, we prefer the mouse lies flat.

13. Obtain a number of imaging planes as shown in Figures 1, 2, and 3. In the short axis view, make sure you have an orthogonal plane of imaging for the most accurate determination of shortening fraction and LV dimensions. Then start with the left parasternal area and obtain a long axis view of the heart to ensure you are orthogonal in the short axis (Figs. 1 and 2A–C).

Approximate transducer positions on the mouse chest are shown in Figure 1.

In the short axis views, the base of the heart can be visualized as one scans more cranially, demonstrating the aortic valve and proximal pulmonary artery (not shown).

The so-called apical 4-chamber view (Fig. 1C) *is difficult to achieve in our experience and others', but one can also image the mitral and aortic valve function in this view* (Fig. 2D and E) *along with spectral Doppler of mitral inflow* (Fig. 2F).

Figure 3 *demonstrates size differences in the parasternal short axis view, as well as our approach to imaging the neonatal mouse*. Figure 4 *demonstrates selected right heart imaging; the reader is referred to a review from Sherrer-Crosbie's group on assessment of murine pulmonary arterial pressures* (Thibault et al., 2010).

14. Perform 2D (or B-mode) imaging.

Typically, 2D imaging alone can be done by one person who can use the foot pedal to freeze the cine loop. However, Doppler interrogation of blood flow will require an additional observer who can place the Doppler sample volume and work the controls.

A typical echocardiogram of a mouse will take under 10 min; several minutes are required for sedation, preparation, and warming to an

appropriate core temperature. The imaging itself, in experienced hands, will take only 1 to 2 min.

15. When imaging is completed, wipe off the gel, remove the mouse from the imaging platform, and place the mouse back in its cage.

16. Monitor all mice post-anesthesia.

    Mice recover from isoflurane within a few minutes, but may take far longer from injectable anesthetics.

17. Perform post-imaging analysis.

    Using the software within the imaging system, we make a number of measurements (detailed in Table 1). *One needs to be careful in the selection of experimental groups: different mouse strains are known to exhibit somewhat different morphologic and functional parameters* (Ram et al., 2011). *It is also preferable that the observer is blinded to the experimental condition to avoid measurement bias.*

Specialized Echocardiographic Techniques

Strain imaging: Speckle-tracking echocardiography—Known also as deformation imaging, echocardiographic strain imaging (Fig. 5) examines myocardial shortening—the extent to which a small region of myocardium shortens, or deforms. This is different from fractional shortening or ejection fraction (see above), which is a measure of change in ventricular cavity size. Speckle tracking is a postprocessing computer algorithm based on the B-mode gray scale tracking of 2D "speckles" or "kernels;" the imaging system essentially tags the myocardium and tracks its motion (in this case, the shortening of a region of myocardium). While strain is the amount (percentage) of deformation, strain rate is the first derivative or the rate (velocity) of deformation, adding additional functional information. Clinical studies have indicated that strain and strain rate imaging are more sensitive to changes in myocardial function (and in particular contractility), while also providing more information on regional wall motion (Gorcsan and Tanaka, 2011; Forsey et al., 2013; Boyd et al., 2015).

High-frequency, small animal ultrasound imaging systems such as the Vevo 2100 have strain and strain rate imaging capabilities. This approach has been applied to mouse models of cardiac dysfunction (for examples, see Peng et al., 2009; Bauer et al., 2011; Bauer et al., 2013; Bhan et al., 2014). Strain and strain rate are typically determined from different views (parasternal long axis, parasternal short axis, apical 4-chamber) and in three directions (longitudinal, radial, and circumferential; Ram et al., 2011). Global as well as regional dysfunction can be determined, and strain indices appear to be more sensitive than traditional indices of global ventricular function such as shortening fraction. In our opinion, validation data are sparse, however. Considerations for strain imaging in mice include:

Images are obtained as for routine B-mode (2D) imaging, from the parasternal windows.

Since strain imaging depends on accurate tracking of speckles or kernels, image quality must be excellent for all segments imaged. The field of view should be coned down to maximize the frame rate (>200 frames/sec), which will help the post-processing algorithm track the echocardiographic speckles. Any shadowing artifact will result in "reduced" strain in the involved (shadowed) segment and lead to an underestimate of global strain, as well as an artifactual "regional wall motion abnormality."

Published experience suggests the parasternal long axis view works well, but not the short axis view. Much of the data in mouse have focused on the utility of longitudinal strain from the parasternal long axis view (Bauer et al., 2011; Bauer et al., 2013; Bhan et al., 2014). We have concerns about the apical segment of the parasternal long axis view (unpublished data). Theoretically, the short axis would be highly valuable in determining regional deformation abnormalities post-myocardial infarction, but obtaining ideal images from all segments remains challenging. The apical 4-chamber view is not useful in mice, since it cannot be obtained as well as in human patients. Figure 5 shows some of our experience with the short axis view.

Pharmacological stress echocardiography—Stress echocardiography images the myocardium during increased oxygen demand imposed by either physical exercise or pharmacological stimulation (Boyd et al., 2015). Stress testing may unveil cardiac dysfunction not apparent at baseline, particularly when a mouse is anesthetized (Bernstein, 2003) and may also exaggerate regional wall motion abnormalities due to ischemia (Boyd et al., 2015). Stress testing in mice is performed using a pharmacological agent such as a β-adrenergic agonist (isoproterenol, dobutamine; see Gao et al., 2011):

We use i.p. isoproterenol (0.2 mg/ml, dissolved in a physiological saline solution such as Hanks balanced salt solution or physiological-buffered saline). Since we inject 0.2 ml per 20 g body weight, this translates into 2 mg/kg.

We then image in the parasternal short axis view for fractional shortening at various time points, typically 1, 3, 5, and 10 min. We find a sharp increase in the heart rate and contractile function within 30 sec post-injection, with near obliteration of the LV cavity. In normal hearts, the increases in cardiac function persist through 10 min, whereas in cardiomyopathic hearts, the responses can be significantly blunted (unpublished data).

Miscellaneous approaches to studying myocardial function—Additional approaches include myocardial contrast echocardiography to measure myocardial perfusion (Scherrer-Crosbie and Kurtz, 2010; Foster et al., 2011; Ram et al., 2011; Moran et al., 2013), elastography to measure regional myocardial function (Luo and Konofagou, 2008), and coronary flow reserve, usually of the left coronary artery under conditions of myocardial damage or stress (Ram et al., 2011; Mercier et al., 2012). The reader is referred to these papers and reviews for further details.

Prenatal Assessment of the Embryonic/Fetal Mouse Cardiovascular System

The advantages of ultrasound/ultrasound biomicroscopy include rapid acquisition times and in vivo imaging with good spatial resolution. However, image contrast tends to be poor relative to other imaging modalities (Norris et al., 2013). Clearly, prenatal cardiovascular imaging of the mouse is far more challenging than postnatal imaging. Gui et al. (1996) first described their technique using a clinical 7 MHz ultrasound system, followed by our lab's approach with a prototype 40 MHz scanner (Srinivasan et al., 1998). With the advent of high-frequency ultrasound imaging systems and probes, arose innovative imaging approaches. Challenges include the far smaller size of the target (mouse embryos or fetuses), the number of mice within the uterine sacs, random orientation of the organism, and movement within the uterus. Although mouse and human heart development are nearly parallel, important differences exist in their overall timelines (Phoon, 2001; Krishnan et al., 2014). Nevertheless, such imaging has been able to address important questions in developmental cardiology and hematology (Phoon, 2006). Although cardiac structures are less often emphasized, our lab (Phoon et al., 2007) and others (Liu et al., 2014) have been able to detect congenital cardiac malformations prenatally.

Materials

Mouse of interest

Isoflurane

Medical oxygen (optional)

Ultrasound (acoustic coupling) gel

Scale (to weigh mouse)

Anesthesia setup

- Anesthetic induction chamber
- Isoflurane distributor
- Mouse anesthesia nosecone delivery system

High-resolution ultrasound imaging system coupled to the anesthesia setup and warming pad that doubles as an imaging platform

Electrocardiography (EKG) system including EKG leads and electrodes (usually incorporated into the imaging platform)

Strips of tape, cut to size (for paws)

Hair dryer (for warm air convection) or warming lamp

1. Perform steps 1 through 10 of Cardiac imaging: Postnatal ultrasound (echocardiography) for neonatal, juveniles, and adults.
2. Once the core temperature is physiological and stable (takes several minutes) with a stable heart rate (Roth et al., 2002), apply the acoustic coupling gel to the abdomen.

In our experience, acoustic coupling gel on the gravid (pregnant) abdomen tends to cool the core temperature far more than when applied to the chest. Therefore, we tend to allow the core temperature to rise to 38°C before application of gel. When gel is applied, the core temperature tends to fall by 1°C.

3. Monitor the pregnant mouse's heart rate to make sure conditions are good for the embryos or fetuses.

Heart rates of sedated mice are typically 400 to 500 bpm. For obvious reasons, we do not image conscious pregnant mice.

4. Begin imaging with a survey of the abdomen. Using the bladder as a reference point, image and follow the uterine horns to either side (Ji and Phoon, 2005).

In experienced hands, one can actually see the vagina, the bifurcation to the uterine horns, and the uterine sacs on each side. One can also then determine whether a mouse is pregnant or not; we find this very useful to efficiently grow colonies or plan prenatal experiments. Mouse embryos/fetuses can be staged as well (Greco et al., 2013).

During early pregnancy (E8.5 to E10.5), the embryos align along either side of the mouse abdomen. As the pregnancy progresses, the uterine sacs will "turn" inward and posteriorly, although often, one can still track embryos/fetuses through about E14.5 to E15.5. Beyond this stage in pregnancy, we believe it becomes impossible to track individual fetuses. Others, too, have acknowledged this challenge (Norris et al., 2013).

Because specific imaging planes are needed, freehand imaging of prenatal mice is the preferred approach. One may need to make minute (<mm) adjustments in transducer positioning (translational, rotational, and angular movements) to achieve the appropriate imaging plane. One must have a very steady hand to image prenatal mice well, and supports for the arms and hands are suggested. A second observer is strongly recommended to work the controls. This way, the imager can focus on the image itself and on keeping track of which embryo is being imaged, while the other observer helps to record and label the images and place the Doppler sample volume as appropriate.

Blood is echogenic up through about E16 to E17 due to nucleated red cells. Therefore, the endocardium is not well-visualized.

5. Obtain a number of imaging planes (see Figs. 6 and 7).

We have relied most on the 4-chamber view (B-mode, color Doppler mapping, and spectral Doppler especially of the AV inflow and aortic outflow), spectral and color Doppler of the dorsal aorta, and spectral and color Doppler of the umbilical vessels (Ji et al., 2003; Phoon et

al., 2004; Nomura-Kitabayashi et al., 2009; Phoon et al., 2012). *Additional information can be obtained from the vitelline circulation* (Phoon and Turnbull, 2003; Phoon, 2006).

A typical echocardiogram of a pregnant mouse will take 30 to 60 min, depending on the number of parameters measured. Several minutes are required for sedation, preparation, and warming to an appropriate core temperature.

6. When imaging is completed, wipe off the gel, remove the mouse from the imaging platform, and place it back in the cage.

7. Monitor all mice post-anesthesia.

8. Perform post-imaging analysis.

Using the software within the imaging system, we make a number of measurements (Table 1). *Preferably, the observer is blinded to the experimental condition in order to avoid measurement bias.*

The Lo lab group has employed a 2-tier approach to screening for cardiac anomalies in a forward mutagenesis screen, using a lower-frequency, clinical ultrasound system for the first level of screening then moving to the Vevo systems for improved resolution. The reader is referred to their papers for details (Liu et al., 2013; Liu et al., 2014).

Newer Technologies: Annular Array Transducers for Fetal Mouse Echocardiography

The technology for in vivo echocardiography in mice has improved significantly in recent years. The commercial scanners now available offer high frequency (30 to 50 MHz) linear array transducers with high spatial and temporal resolution for improved dynamic and functional analyses. Despite these advances, the current linear array transducers still present limitations in spatial resolution, especially in the elevation (out-of-plane) direction, where the width of the ultrasound beam is significantly larger than in the azimuthal (in-plane) direction. This can be problematic for analyses of very small cardiovascular structures in mouse embryos, especially at earlier stages (E10.5 to E14.5) when many morphological and functional changes occur and when many cardiac-specific phenotypes are first manifested in mutant embryos. These considerations have led us investigate the utility of annular array transducers that provide axi-symmetric focusing, integrated into scanners with 3D image acquisition more suitable for in utero studies of developing mouse embryos (Aristizábal et al., 2006; Aristizábal et al., 2013).

Quantitative comparisons of imaging performance in phantoms designed to detect these differences have clearly shown that axi-symmetrically focused annular array transducers have superior spatial resolution compared to commercially available linear arrays (Filoux et al., 2011; Filoux et al., 2012). These gains in resolution have translated into improved capability for 3D in utero analyses of brain development (Aristizábal et al., 2013). Since the annular array transducers cannot be used to steer the beam off axis, they must be mechanically scanned to acquire 2D and 3D image data, which necessitates motion-gated acquisition, similar to most MRI methods. Respiratory-gated ultrasound biomicroscopy

(UBM) was shown to be sufficient for high-throughput 3D fetal brain imaging (Aristizábal et al., 2013), but 3D imaging of the beating mouse heart will require combined respiratory and cardiac gating (Ketterling and Aristizábal, 2009). In the case of in utero echocardiography, where an EKG signal is not available, it is possible to employ a Doppler ultrasound signal as the trigger for cardiac gating (Aristizábal et al., 2009).

VASCULAR IMAGING: ULTRASOUND

Vascular imaging is valuable in mouse models of atherosclerosis, vascular interventions, or to determine the success (degree) of transverse aortic constriction (Hartley et al., 2011; Ram et al., 2011). Atherosclerotic lesions, an abnormally thickened intima-media layer, and vascular thromboses may be directly imaged with high resolution ultrasound (Choudhury et al., 2004; Chatterjee et al., 2014; Zhang et al., 2015) and also enhanced with specific contrast agents (Wang et al., 2012; Foss et al., 2015). Arterial stiffness may be determined by the pulse wave velocity (Hartley et al., 2011; Chatterjee et al., 2014) or a combination of aortic diameter and invasive blood pressure measurements (Kuo et al., 2014); for a more precise determination of localized arterial wall characteristics, pulse wave imaging has more recently been developed (Fujikura et al., 2007; Nandlall et al., 2014). Similarly, arterial wall strain may now be measured, as well (Favreau et al., 2014). To achieve the highest B-mode resolution images in general, the long axis of the vessel should be approximately orthogonal to the ultrasound beam; in contrast, Doppler beams must be placed as close to parallel to the artery as possible. Representative images from our lab of the normal aorta, aortic arch, and carotid artery are shown in Figure 8.

CARDIOVASCULAR MRI

MRI is now used for cardiac and vascular imaging in many human patients, although generally as a secondary modality following an initial exam with echocardiography. Over the past decade, dedicated high-field (≥7 Tesla) MRI systems have become more common for small animal imaging, and many biologists now consider incorporating MRI into studies of the mouse cardiovascular system. Traditional MRI images derive tissue contrast from differences in proton density, T1 or T2 relaxation times, but other methods also are available to show differences in diffusion, perfusion, or blood flow. This makes MRI a very flexible imaging modality compared to echocardiography, with many options for manipulating image contrast. MRI offers additional advantages over echocardiography including intrinsic three-dimensional image acquisition along image-defined projections so that assumptions about LV geometry do not need to be made (as is often the case with echocardiography) and the ability to study many pathophysiological parameters in a single session, including energy metabolism (Akki et al., 2013). Despite these apparent advantages, it must be recognized that MRI in mice, especially at fetal and neonatal stages, is very challenging due to the small size of the cardiac chambers and blood vessels, the rapid heart rates, and the short T2 relaxation times at high field strengths. For most biologists, cardiac MRI can only be successfully undertaken in collaboration with a team that specializes in these approaches.

Cardiac MRI offers similar capabilities and advantages as echocardiography: cine MRI for in vivo and longitudinal measurements of LV size, shape, and wall thickening at relatively

high spatial resolution (~100 μm isotropic); strain imaging via myocardial tagging; and myocardial perfusion studies via arterial spin labeling or dynamic contrast-enhanced MRI (reviewed in Epstein, 2007). Contrast agent-enhanced studies can also be employed to assess myocardial infarction and for molecular imaging with targeted contrast agents (reviewed in Epstein, 2007; Vandsburger and Epstein, 2011). Moreover, MR spectroscopy permits the study of cardiac metabolism, both in vivo and in the isolated perfused heart (Epstein, 2007; Akki et al., 2013). Unlike echocardiography, most cardiac MRI approaches are not real time. Rather, MRI data are acquired using gating methods over a number of heartbeats, with the implicit assumption that each cardiac cycle is similar to the previous. Cardiac MRI often complements echocardiography for certain pathophysiological questions, such as post-myocardial infarct healing (Gray et al., 2013). Below, we sketch out the main requirements for cardiovascular MRI in mice at both postnatal and fetal stages.

In Vivo MRI of Mice

Mice must be maintained under anesthesia, and their physiological status carefully maintained and monitored during in vivo MRI acquisitions, which are often performed for extended time periods up to ~3 hr. During this time, the mouse is secured in a holder (usually custom made) designed to facilitate anesthesia gas delivery, physiological monitoring, and reproducible positioning within the radiofrequency (RF) coil that acquires the MRI data. Isoflurane gas is most commonly used for anesthesia in mice (induced with 4% to 5% and maintained at ~1.0% isoflurane in air). For cardiovascular imaging, it is important that core temperature (monitored with a rectal temperature probe) be maintained close to 37°C using circulated warm water or air. EKG electrodes are typically incorporated into the mouse holder to monitor heart rate and to provide the trigger signal for cardiac-gated acquisition. A respiratory pillow can be used to monitor the breathing rate. Reliable EKG and respiratory signals can be very difficult to obtain in early postnatal mice, and we prefer to use modified “self-gated” pulse sequences that detect respiratory and/or cardiac motion directly from the acquired MRI signals (Nieman et al., 2009).

For in utero MRI it is impossible to use external devices to detect fetal motion. Instead, we employ a self-gated gradient echo sequence—sensitive to the endogenous contrast of the embryonic mouse blood—together with image co-registration to obtain 3D cine images of the beating heart (Nieman et al., 2009; Fig. 9) and cerebral vasculature (Berrios-Otero et al., 2012; Parasoglou et al., 2013). More specialized pulse sequences would be required for strain imaging and perfusion studies, but, in principle, any existing pulse sequence could be modified to incorporate self-gating for motion compensation. In practice, in utero images have a very limited signal-to-noise ratio (SNR), and more specialized cardiac MRI studies have not been demonstrated in mouse embryos. In future, dedicated hardware and software will be required for improved in utero imaging in mice. In particular, improved RF coil arrays for small animal MRI might enable extended field-of-view (FOV) images to map out the position of multiple embryos, followed by single-coil small FOV images of individual embryos. Coil arrays for parallel imaging could also be combined with sparse data reconstruction (compressed sensing) methods, to accelerate image acquisition and/or improve SNR as recently reported in adult mouse cardiac MRI (Prieto et al., 2012; Buonincontri et al., 2014).

Ex Vivo MRI of Fixed Samples

Although MRI is often considered because of its potential for in vivo imaging, it can also be used for nondestructive ex vivo imaging of fixed tissues. This approach has been utilized extensively for studies of embryonic cardiovascular development, dating back to the pioneering reports of Smith, Johnson, and co-workers (Smith et al., 1994; reviewed in Smith, 2001). Although functional studies of cardiac dynamics and blood flow studies are obviously not possible, ex vivo MRI has been very useful for analyzing cardiac and large vessel structural phenotypes in mutant mouse embryos (Huang et al., 1998; Bamforth et al., 2004; Wadghiri et al., 2007; reviewed in Turnbull and Mori, 2007; Nieman and Turnbull, 2010). Ex vivo MRI is inherently motion free, and scans are generally run overnight for many hours to obtain high-resolution (20 to 50 μm isotropic) 3D images. A number of centers have implemented multiple-sample overnight ex vivo imaging, making use of otherwise unused scanner time and providing high-throughput approaches for screening new mutant mice at defined developmental stages (Schneider et al., 2004; Zhang et al., 2010; reviewed in Nieman and Turnbull, 2010).

For ex vivo MRI, mice are euthanized and tissue samples are dissected, fixed, and mounted in the RF coil for imaging (Dhenain et al., 2001). For vascular imaging in mid- to late-stage embryonic mice, perfusion fixation is preferred, using a contrast agent solution to preferentially enhance the vasculature and performing imaging on the whole embryo (see below). For ex vivo MRI, fixed embryos or tissue samples are immersed in 4% paraformaldehyde in PBS overnight (or longer) at 4°C, after which they can be stored in PBS. The fixative and/or storage medium is often “doped” with an MRI contrast agent, usually a chelated gadolinium (Gd) compound such as DTPA-Gd or DOTA-Gd (2 to 3 mM concentration in the fixative), to increase the SNR of the resulting T2-weighted MRI images (Petiet et al., 2008). For imaging, the samples are embedded in 1% to 3% agar, or immersed in proton-free fluid (Fomblin or Fluorinert) to reduce the background signal. Samples are then placed within a close-fitting RF coil for ex vivo MRI.

Perfusion Fixation with Contrast Agents for Ex Vivo MRI

For ex vivo MRI of embryonic vasculature, we employ protocols similar to those first described by Smith and co-workers (Smith, 2000; Smith et al., 1994). Timed pregnant mice (where E0.5 denotes noon of the day after overnight breeding) are anesthetized and the uterus accessed through laparotomy. Individual embryos are surgically removed from the uterus, maintaining the vascular connections to the placenta and warmed in 37°C PBS to keep the heart beating normally at the start of the perfusion. Under a dissection microscope, the umbilical vein is identified and cannulated with a pulled glass microcapillary needle, and the embryo is perfused with a slow flow rate (~0.1 to 0.15 ml/min) pump: (1) starting with warm PBS containing heparin (5000 U/liter); (2) followed by fixative (2% [v/v] glutaraldehyde, 1% [v/v] formalin in PBS); and (3) finally followed by the contrast agent, bovine serum albumin (BSA) conjugated to DTPA-Gd (BSA-DTPA-Gd; 1 mM) dissolved in 10% (w/v) gelatin solution. For full perfusion of all blood vessels, the umbilical vein is used for all three perfusates; when selective enhancement of the cerebral arteries was desired, we found that a timed perfusion of the contrast agent through the umbilical artery worked best (Berrios-Otero et al., 2009; Fig. 10). Recently, a novel approach for contrast-enhanced

micro-CT has been shown to generate more complete cerebral vascular filling by directing the contrast agent through the posterior brain arteries (Ghanavati et al., 2014), a method that could easily be adopted for ex vivo MRI. After perfusion, the umbilical vessels are ligated, and the samples are immersed in 4°C fixative to solidify the gelatin and completely fix the tissue. Ex vivo MRI is then performed on the fixed embryos, as described above.

Image Analysis Methods

Although we have focused on the acquisition of ultrasound and MRI data related to cardiovascular structure and function, data analysis is an equally important subject, but one that will only be discussed briefly here. Most work to date has relied on qualitative observations from 2D and 3D images and rudimentary quantitative analysis of anatomical (e.g., LV area, volume) and functional (e.g., peak blood velocity, ejection fraction) parameters. Several groups are developing automated registration-based ex vivo MRI morphometry approaches for cardiovascular phenotype analysis in mutant mice (Zamyadi et al., 2010). While simple measurements of isolated geometric factors (branch length and angles) in complex vascular trees may suffice to characterize obvious defects in vascular patterns (Berrios-Otero et al., 2009), ultimately a more systematic and automated approach is required to detect and characterize subtle (non-lethal) vascular phenotypes (Dorr et al., 2007) on both the structural and functional levels (Yang et al., 2010; Ghanavati et al., 2014).

Molecular Imaging of Vasculature

Like ultrasound, MRI can also provide information on vascular biology, including mouse models of atherosclerosis (Millon et al., 2014). For phenotype analysis in mouse models, combined structural, functional, and molecular imaging has the potential to provide a more complete picture of the complex molecular and mechanical events driving cardiovascular development and disease. Molecular imaging of mouse vasculature has been demonstrated with both ultrasound (reviewed in Lindner, 2010) and MRI (reviewed in Artemov et al., 2004), using intravascular injection of contrast agents (microbubbles for ultrasound; Gd chelates or iron oxide nanoparticles for MRI) that are targeted to receptors on the surface of vascular endothelial cells via receptor-ligand binding. Notably, $\alpha_v\beta_3$-integrin and VEGFR2, which are highly expressed in tumors and vascular pathologies, have both been reported as viable targets for molecular imaging with MRI and ultrasound. Unfortunately, receptor-ligand binding affinities are relatively low and can be limiting in the presence of shear forces associated with blood flows in the cardiovascular system. Moreover, targeted imaging as described above is limited to extracellular proteins, leaving many intracellular molecules inaccessible to imaging studies.

To address these limitations in current molecular imaging technology, we developed a novel “Biotag” transgene for biotinylation of cell membranes, allowing them to be targeted with (strept)avidinated contrast agents (Bartelle et al., 2012; Fig. 11). The Biotag transgene can be used for molecular imaging of vasculature with ultrasound and MRI (and other imaging modalities) and has been demonstrated to be an effective approach in both embryonic and adult models of angiogenesis. Biotag expression, and subsequent membrane biotinylation, can be driven from the regulatory elements of any gene by generating the appropriate transgenic or knock-in mouse reporter line, making it possible to extend molecular imaging

to a wide variety of genetic factors involved in vascular development and disease. Future development of other expressible reporters that can be detected with MRI and/or ultrasound will likely have a significant impact on the use of cardiovascular imaging in mouse models.

ADDITIONAL SPECIALIZED CARDIOVASCULAR IMAGING APPROACHES

Optical Coherence Tomography

Optical coherence tomography (OCT) is conceptually analogous to ultrasound, except that it measures the echo time delay and magnitude of light instead of ultrasound (Fujimoto, 2003). Because optical echoes cannot be measured directly due to the speed of light, OCT uses coherence interferometry instead to obtain data which can be used to then generate an image (Fujimoto, 2003; Garcia et al., 2015). Advantages of OCT include very high spatial resolution—in the micron to submicron range—using state-of-the-art laser technology. However, there is a trade-off with depth of penetration in the range of 2 to 3 mm only, due to signal attenuation and scattering (Fujimoto, 2003; Drexler et al., 2014; Garcia et al., 2015). Although OCT has been used more extensively in non-mammalian model systems, this shallow depth of penetration limits its utility in mouse cardiovascular imaging, where much of the work has focused on imaging of cultured mouse embryonic hemodynamics during development (Larina et al., 2008; Larina et al., 2011; Larina et al., 2012; Garcia et al., 2015), although in utero imaging is feasible (Larina et al., 2011). More recently, techniques have been developed for imaging of (isolated Langendorff) adult mouse hearts by implementing multiperspective imaging and optical clearing that permit insights into tissue characteristics (Cua et al., 2014). The imaging approaches outlined above are not in vivo, but recent reports suggest utility of OCT as an intravital vascular imaging modality, specifically in a mouse hind limb ischemia model (Poole et al., 2013).

Optical Projection Tomography

Optical projection tomography (OPT) fills a niche that allows high-resolution imaging of whole mouse embryos (Sharpe et al., 2002). From an emitted, focused light source and rotated sample, OPT utilizes projection tomography and in situ immunostains to generate a three-dimensional image of a whole embryo's gene expression patterns. OPT has been utilized for imaging the developing cardiovascular system and particularly the developing vasculature ex vivo (Ruijter et al., 2004; Walls et al., 2008; Anderson et al., 2013). Most OPT has been performed on fixed and optically cleared specimens, but more recently, live OPT imaging has been achieved (Colas and Sharpe, 2009). Live cardiovascular imaging of the developing mouse embryo is still at rudimentary stages, however, and the next challenges are to overcome imaging artifacts inherent in cardiac motion (Colas and Sharp, 2009). In the adult mouse heart, a Born-normalized near-infrared fluorescence OPT imaging system has been more recently described, which allows imaging of spatiotemporal dynamics of diverse cells by quantitating and resolving molecular agents within the imaged heart (Vinegoni et al., 2012).

Live Confocal Microscopy

Cultured mouse embryos have also been imaged with live confocal microscopy. Specifically, the yolk sac vasculature of the developing mouse embryo can be interrogated to characterize

evolving hemodynamics that contribute to overall mouse cardiovascular development (Lopez et al., 2015).

Acknowledgments

The authors would like to thank members of the Phoon and Turnbull labs over the years for their input and assistance on the innovative imaging approaches developed. Work was supported by NIH grants R01HL078665 and R01NS038461 (DHT). The Vevo 2100 ultrasound imaging system at NYU Langone Medical Center was supported by NIH grant 1S10RR026881. The Small Animal Imaging Core at NYU Langone Medical Center assisted in this work and is supported in part by NIH grants P30CA016087 (to NYU Cancer Institute) and UL1TR00038 (to NYU Clinical and Translational Science Institute).

LITERATURE CITED

Adams D, Baldock R, Bhattacharya S, Copp AJ, Dickinson M, Greene ND, Henkelman M, Justice M, Mohun T, Murray SA, Pauws E, Raess M, Rossant J, Weaver T, West D. Bloomsbury report on mouse embryo phenotyping: Recommendations from the IMPC workshop on embryonic lethal screening. Dis Model Mech. 2013; 6:571–579. DOI: 10.1242/dmm.011833 [PubMed: 23519032]

Akki A, Gupta A, Weiss RG. Magnetic resonance imaging and spectroscopy of the murine cardiovascular system. Am J Physiol Heart Circ Physiol. 2013; 304:H633–H648. [PubMed: 23292717]

Anderson GA, Wong MD, Yang J, Henkelman RM. 3D imaging, registration, and analysis of the early mouse embryonic vasculature. Dev Dynam. 2013; 242:527–538. DOI: 10.1002/dvdy.23947

Aristizábal O, Ketterling JA, Turnbull DH. 40-MHz annular array imaging of mouse embryos. Ultrasound Med Biol. 2006; 32:1631–1637. DOI: 10.1016/j.ultrasmedbio.2006.05.020 [PubMed: 17112949]

Aristizábal O, Mamou J, Turnbull DH, Ketterling JA. Doppler-derived trigger signals for high-frame-rate mouse cardiovascular imaging. Conf Proc IEEE Eng Med Biol Soc. 2009; 1:1987–1990. [PubMed: 19964029]

Aristizábal O, Mamou J, Ketterling JA, Turnbull DH. High-throughput, high-frequency 3-D ultrasound for in utero analysis of embryonic mouse brain development. Ultrasound Med Biol. 2013; 39:2321–2332. DOI: 10.1016/j.ultrasmedbio.2013.06.015 [PubMed: 24035625]

Artemov D, Bhujwalla ZM, Bulte JW. Magnetic resonance imaging of cell surface receptors using targeted contrast agents. Curr Pharm Biotechnol. 2004; 5:485–494. DOI: 10.2174/1389201043376553 [PubMed: 15579038]

Bamforth SD, Bragança J, Farthing CR, Schneider JE, Broadbent C, Michell AC, Clarke K, Neubauer S, Norris D, Brown NA, Anderson RH, Bhattacharya S. Cited2 controls left-right patterning and heart development through a Nodal-Pitx2c pathway. Nat Genet. 2004; 36:1189–1196. DOI: 10.1038/ng1446 [PubMed: 15475956]

Bartelle BB, Berrios-Otero CA, Rodriguez JJ, Friedland AE, Aristizábal O, Turnbull DH. Novel genetic approach for in vivo vascular imaging in mice. Circ Res. 2012; 110:938–947. DOI: 10.1161/CIRCRESAHA.111.254375 [PubMed: 22374133]

Bauer M, Cheng S, Unno K, Lin F-C, Liao R. Regional cardiac dysfunction and dyssynchrony in a murine model of afterload stress. PLoS One. 2013; 8:e59915.doi: 10.1371/journal.pone.0059915 [PubMed: 23560059]

Bauer M, Cheng S, Jain M, Ngoy S, Theodoropoulos C, Trujillo A, Lin F-C, Liao R. Echocardiographic speckle-tracking based strain imaging for rapid cardiovascular phenotyping in mice. Circ Res. 2011; 108:908–916. DOI: 10.1161/CIRCRESAHA.110.239574 [PubMed: 21372284]

Bernstein D. Exercise assessment of transgenic models of human cardiovascular disease. Physiol Genomics. 2003; 13:217–226. DOI: 10.1152/physiolgenomics.00188.2002 [PubMed: 12746466]

Berrios-Otero CA, Nieman BJ, Parasoglou P, Turnbull DH. In utero phenotyping of mouse embryonic vasculature with MRI. Magn Reson Med. 2012; 67:251–257. DOI: 10.1002/mrm.22991 [PubMed: 21590728]

Berrios-Otero CA, Wadghiri YZ, Nieman BJ, Joyner AL, Turnbull DH. Three-dimensional micro-MRI analysis of cerebral artery development in mouse embryos. Magn Reson Med. 2009; 62:1431–1439. DOI: 10.1002/mrm.22113 [PubMed: 19859945]

Berry CJ, Thedens DR, Light-McGroary K, Miller JD, Kutschke W, Zimmerman KA, Weiss RM. Effects of deep sedation or general anesthesia on cardiac function in mice undergoing cardiovascular magnetic resonance. J Cardiovasc Magn Reson. 2009; 11:16.doi: 10.1186/1532-429X-11-16 [PubMed: 19454023]

Bhan A, Sirker A, Zhang J, Protti A, Catibog N, Driver W, Botnar R, Monaghan MJ, Shah AM. High-frequency speckle tracking echocardiography in the assessment of left ventricular function and remodeling after murine myocardial infarction. Am J Physiol Heart Circ Physiol. 2014; 306:H1371–H1383. DOI: 10.1152/ajpheart.00553.2013 [PubMed: 24531814]

Boyd AC, Schiller NB, Thomas L. Principles of transthoracic echocardiographic evaluation. Nat Rev Cardiol. 2015; 12:426–440. DOI: 10.1038/nrcardio.2015.57 [PubMed: 25917151]

Buonincontri G, Methner C, Krieg T, Carpenter TA, Sawiak SJ. Functional assessment of the mouse heart by MRI with a 1-min acquisition. NMR Biomed. 2014; 27:733–737. DOI: 10.1002/nbm.3116 [PubMed: 24737267]

Chatterjee S, Bedja D, Mishra S, Amuzie C, Avolio A, Kass DA, Berkowitz D, Renehan M. Inhibition of glycosphingolipid synthesis ameliorates atherosclerosis and arterial stiffness in apolipoprotein E −/− mice and rabbits fed a high-fat and -cholesterol diet. Circulation. 2014; 129:2403–2413. DOI: 10.1161/CIRCULATIONAHA.113.007559 [PubMed: 24710030]

Choudhury RP, Fuster V, Fayad ZA. Molecular, cellular and functional imaging of atherothrombosis. Nat Rev Drug Discov. 2004; 3:913–925. DOI: 10.1038/nrd1548 [PubMed: 15520814]

Colas JF, Sharpe J. Live optical projection tomography. Organogenesis. 2009; 5:211–216. DOI: 10.4161/org.5.4.10426 [PubMed: 20539740]

Collis LP, Meyers MB, Zhang J, Phoon CKL, Sobie EA, Coetzee WA, Fishman GI. Expression of a sorcin missense mutation in the heart modulates excitation-contraction coupling. FASEB J. 2007; 21:475–487. DOI: 10.1096/fj.06-6292com [PubMed: 17130302]

Cua M, Lin E, Lee L, Sheng X, Wong KS, Tibbits GF, Beg MF, Sarunic MV. Morphological phenotyping of mouse hearts using optical coherence tomography. J Biomed Opt. 2014; 19:116007.doi: 10.1117/1.JBO.19.11.116007 [PubMed: 25393967]

Danielson LS, Park DS, Rotllan N, Chamorro-Jorganes A, Guijarro MV, Fernandez-Hernando C, Fishman GI, Phoon CKL, Hernando E. Cardiovascular dysregulation of miR-17–92 causes a lethal hypertrophic cardiomyopathy and arrhythmogenesis. FASEB J. 2013; 27:1460–1467. DOI: 10.1096/fj.12-221994 [PubMed: 23271053]

Dhenain M, Ruffins SW, Jacobs RE. Three-dimensional digital mouse atlas using high-resolution MRI. Dev Biol. 2001; 232:458–470. DOI: 10.1006/dbio.2001.0189 [PubMed: 11401405]

Dorr A, Sled JG, Kabani N. Three-dimensional cerebral vasculature of the CBA mouse brain: A magnetic resonance imaging and micro computed tomography study. Neuroimage. 2007; 35:1409–1423. DOI: 10.1016/j.neuroimage.2006.12.040 [PubMed: 17369055]

Drexler W, Liu M, Kumar A, Kamali T, Unterhuber A, Leitgeb RA. Optical coherence tomography today: Speed, contrast, and multimodality. J Biomed Opt. 2014; 19:071412.doi: 10.1117/1.JBO.19.7.071412 [PubMed: 25079820]

Epstein FH. MR in mouse models of cardiac disease. NMR Biomed. 2007; 20:238–255. DOI: 10.1002/nbm.1152 [PubMed: 17451182]

Favreau JT, Liu C, Yu P, Tao M, Mauro C, Gaudette GR, Ozaki CK. Acute reductions in mechanical wall strain precede the formation of intimal hyperplasia in a murine model of arterial occlusive disease. J Vasc Surg. 2014; 60:1340–1347. DOI: 10.1016/j.jvs.2013.07.113 [PubMed: 24139980]

Fayssoil A, Tournoux F. Analyzing left ventricular function in mice with Doppler echocardiography. Heart Fail Rev. 2013; 18:511–516. DOI: 10.1007/s10741-012-9345-8 [PubMed: 22961495]

Filoux E, Mamou J, Aristizábal O, Ketterling JA. Characterization of the spatial resolution of different high-frequency imaging systems using a novel anechoic-sphere phantom. IEEE Trans Ultrason Ferroelectr Freq Control. 2011; 58:994–1005. [PubMed: 21622055]

Filoux E, Mamou J, Moran CM, Pye SD, Ketterling JA. Correspondence - Characterization of the effective performance of a high-frequency annular-array-based imaging system using anechoic-

pipe phantoms. IEEE Trans Ultrason Ferroelectr Freq Control. 2012; 59:2825–2830. DOI: 10.1109/TED.2012.2209650 [PubMed: 23221233]

Forsey J, Friedberg MK, Mertens L. Speckle tracking echocardiography in pediatric and congenital heart disease. Echocardiography. 2013; 30:447–459. DOI: 10.1111/echo.12131 [PubMed: 23551605]

Foss CA, Bedja D, Mease RC, Wang H, Kass DA, Chatterjee S, Pomper MG. Molecular imaging of inflammation in the ApoE−/− mouse model of atherosclerosis with IodoDPA. Biochem Biophys Res Commun. 2015; 461:70–75. DOI: 10.1016/j.bbrc.2015.03.171 [PubMed: 25858322]

Foster FS, Hossack J, Adamson SL. Micro-ultrasound for preclinical imaging. Interface Focus. 2011; 1:576–601. DOI: 10.1098/rsfs.2011.0037 [PubMed: 22866232]

Fujikura K, Luo J, Gamarnik V, Pernot M, Fukumoto R, Tilson MD 3rd, Konofagou EE. A novel noninvasive technique for pulse-wave imaging and characterization of clinically-significant vascular mechanical properties in vivo. Ultrason Imaging. 2007; 29:137–154. DOI: 10.1177/016173460702900301 [PubMed: 18092671]

Fujimoto JG. Optical coherence tomography for ultrahigh resolution in vivo imaging. Nat Biotech. 2003; 21:1361–1367. DOI: 10.1038/nbt892

Gao S, Ho D, Vatner DE, Vatner SF. Echocardiography in mice. Curr Protocols Mouse Biol. 2011; 1:71–83.

Garcia MD, Lopez AL 3rd, Larin KV, Larina IV. Imaging of cardiovascular development in mammalian embryos using optical coherence tomography. Methods Mol Biol. 2015; 1214:151–161. DOI: 10.1007/978-1-4939-1462-3_8 [PubMed: 25468602]

Gardin JM, Siri FM, Kitsis RN, Edwards JG, Leinwand LA. Echocardiographic assessment of left ventricular mass and systolic function in mice. Circ Res. 1995; 76:907–914. DOI: 10.1161/01.RES.76.5.907 [PubMed: 7729009]

Ghanavati S, Lerch JP, Sled JG. Automatic anatomical labeling of the complete cerebral vasculature in mouse models. Neuroimage. 2014; 95:117–128. DOI: 10.1016/j.neuroimage.2014.03.044 [PubMed: 24680868]

Ghanavati S, Yu LX, Lerch JP, Sled JG. A perfusion procedure for imaging of the mouse cerebral vasculature by X-ray micro-CT. J Neurosci Methods. 2014; 221:70–77. DOI: 10.1016/j.jneumeth.2013.09.002 [PubMed: 24056228]

Gorcsan J 3rd, Tanaka H. Echocardiographic assessment of myocardial strain. J Am Coll Cardiol. 2011; 58:1401–1413. DOI: 10.1016/j.jacc.2011.06.038 [PubMed: 21939821]

Gray GA, White CI, Thomson A, Kozak A, Moran C, Jansen MA. Imaging the healing murine myocardial infarct in vivo: Ultrasound, magnetic resonance imaging and fluorescence molecular tomography. Exp Physiol. 2013; 98:606–613. DOI: 10.1113/expphysiol.2012.064741 [PubMed: 23064510]

Greco A, Ragucci M, Coda AR, Rosa A, Gargiulo S, Liuzzi R, Gramanzini M, Albanese S, Pappatà S, Mancini M, Brunetti A, Salvatore M. High frequency ultrasound for in vivo pregnancy diagnosis and staging of placental and fetal development in mice. PLoS One. 2013; 8:e77205.doi: 10.1371/journal.pone.0077205 [PubMed: 24155928]

Gui YH, Linask KK, Khowsathit P, Huhta JC. Doppler echocardiography of normal and abnormal embryonic mouse heart. Pediatr Res. 1996; 40:633–642. DOI: 10.1203/00006450-199610000-00020 [PubMed: 8888295]

Hartley CJ, Reddy AK, Madala S, Entman ml, Michael LH, Taffet GE. Doppler velocity measurements from large and small arteries of mice. Am J Physiol Heart Circ Physiol. 2011; 301:H269–278. DOI: 10.1152/ajpheart.00320.2011 [PubMed: 21572013]

Hoffman JIE. Incidence of congenital heart disease: II. Prenatal incidence. Pediatr Cardiol. 1995; 16:155–165. [PubMed: 7567659]

Hoffman JIE, Kaplan S. The incidence of congenital heart disease. J Am Coll Cardiol. 2002; 39:1890–1900. DOI: 10.1016/S0735-1097(02)01886-7 [PubMed: 12084585]

Huang GY, Wessels A, Smith BR, Linask KK, Ewart JL, Lo CW. Alteration in connexin 43 gap junction gene dosage impairs conotruncal heart development. Dev Biol. 1998; 198:32–44. DOI: 10.1006/dbio.1998.8891 [PubMed: 9640330]

Ji RP, Phoon CKL. Non-invasive localization of NFATc1−/− mouse embryos by ultrasound biomicroscopy-Doppler allows genotype-phenotype correlation. J Am Soc Echocardiogr. 2005; 18:1415–1421. DOI: 10.1016/j.echo.2005.04.006 [PubMed: 16376776]

Ji RP, Phoon CKL, Aristizábal O, McGrath KE, Palis J, Turnbull DH. Onset of cardiac function during early mouse embryogenesis coincides with entry of primitive erythroblasts into the embryo proper. Circ Res. 2003; 92:133–135. DOI: 10.1161/01.RES.0000056532.18710.C0 [PubMed: 12574139]

Ketterling JA, Aristizábal O. Prospective ECG-gated mouse cardiac imaging with a 34-MHz annular array transducer. IEEE Trans Ultrason Ferroelectr Freq Control. 2009; 56:1394–1404. [PubMed: 19574150]

Kober F, Iltis I, Cozzone PJ, Bernard M. Cine-MRI assessment of cardiac function in mice anesthetized with ketamine/xylazine and isoflurane. MAGMA. 2004; 17:157–161. DOI: 10.1007/s10334-004-0086-0 [PubMed: 15609036]

Krishnan A, Samtani R, Dhanantwari P, Lee E, Yamada S, Shiota K, Donofrio MT, Leatherbury L, Lo CW. A detailed comparison of mouse and human cardiac development. Pediatr Res. 2014; 76:500–507. DOI: 10.1038/pr.2014.128 [PubMed: 25167202]

Kuo MM, Barodka V, Abraham TP, Steppan J, Shoukas AA, Butlin M, Avolio A, Berkowitz DE, Santhanam L. Measuring ascending aortic stiffness in vivo in mice using ultrasound. J Vis Exp. 2014; 94:e52200.doi: 10.3791/52200

Larina IV, Larin KV, Justice MV, Dickinson ME. Optical coherence tomography for live imaging of mammalian development. Curr Opin Genet Dev. 2011; 21:579–584. DOI: 10.1016/j.gde.2011.09.004 [PubMed: 21962442]

Larina IV, Garcia MD, Vadakkan TJ, Larin KV, Dickinson ME. Imaging mouse embryonic cardiovascular development. Cold Spring Harb Protoc. 2012; 2012:1035–1043. DOI: 10.1101/pdb.top071498 [PubMed: 23028074]

Larina IV, Sudheendran N, Ghosn M, Jiang J, Cable A, Larin KV, Dickinson ME. Live imaging of blood flow in mammalian embryos using Doppler swept-source optical coherence tomography. J Biomed Opt. 2008; 13:060506.doi: 10.1117/1.3046716 [PubMed: 19123647]

Lindner JR. Molecular imaging of myocardial and vascular disorders with ultrasound. JACC Cardiovasc Imaging. 2010; 3:204–211. DOI: 10.1016/j.jcmg.2009.09.021 [PubMed: 20159648]

Liu J, Rigel DF. Echocardiographic examination in rats and mice. Methods Mol Biol. 2009; 573:139–155. DOI: 10.1007/978-1-60761-247-6_8 [PubMed: 19763926]

Liu X, Tobita K, Francis RJ, Lo CW. Imaging techniques for visualizing and phenotyping congenital heart defects in murine models. Birth Defects Res C Embryo Today. 2013; 99:93–105. DOI: 10.1002/bdrc.21037 [PubMed: 23897594]

Liu X, Francis R, Kim AJ, Ramirez R, Chen G, Subramanian R, Anderton S, Kim Y, Wong L, Morgan J, Pratt HC, Reinholdt L, Devine W, Leatherbury L, Tobita K, Lo CW. Interrogating congenital heart defects with noninvasive fetal echocardiography in a mouse forward genetic screen. Circ Cardiovasc Imaging. 2014; 7:31–42. DOI: 10.1161/CIRCIMAGING.113.000451 [PubMed: 24319090]

Lopez AL 3rd, Garcia MD, Dickinson ME, Larina IV. Live confocal microscopy of the developing mouse embryonic yolk sac vasculature. Methods Mol Biol. 2015; 1214:163–172. DOI: 10.1007/978-1-4939-1462-3_9 [PubMed: 25468603]

Luo J, Konofagou EE. High-frame rate, full-view myocardial elastography with automated contour tracking in murine left ventricles in vivo. IEEE Trans Ultrason Ferroelectr Freq Control. 2008; 55:240–248. DOI: 10.1109/TUFFC.2008.633 [PubMed: 18334330]

Manning WJ, Wei JY, Katz SE, Litwin SE, Douglas PS. In vivo assessment of LV mass in mice using high-frequency cardiac ultrasound: Necropsy validation. Am J Physiol. 1994; 266:H1672–675. [PubMed: 8184946]

Mercier N, Kiviniemi TO, Saraste A, Miiluniemi M, Silvola J, Jalkanen S, Yegutkin GG. Impaired ATP-induced coronary blood flow and diminished aortic NTPDase activity precede lesion formation in apolipoprotein E-deficient mice. Am J Pathol. 2012; 180:419–428. DOI: 10.1016/j.ajpath.2011.10.002 [PubMed: 22074736]

Millon A, Canet-Soulas E, Boussel L, Fayad Z, Douek P. Animal models of atherosclerosis and magnetic resonance imaging for monitoring plaque progression. Vascular. 2014; 22:221–237. DOI: 10.1177/1708538113478758 [PubMed: 24907292]

Moran CM, Thomson AJW, Rog-Zielinska E, Gray GA. High-resolution echocardiography in the assessment of cardiac physiology and disease in preclinical models. Exp Physiol. 2013; 98:629–644. DOI: 10.1113/expphysiol.2012.068577 [PubMed: 23118017]

Mozaffarian D, Benjamin EJ, Go AS, Arnett DK, Blaha MJ, Cushman M, de Ferranti S, Després JP, Fullerton HJ, Howard VJ, Huffman MD, Judd SE, Kissela BM, Lackland DT, Lichtman JH, Lisabeth LD, Liu S, Mackey RH, Matchar DB, McGuire DK, Mohler ER 3rd, Moy CS, Muntner P, Mussolino ME, Nasir K, Neumar RW, Nichol G, Palaniappan L, Pandey DK, Reeves MJ, Rodriguez CJ, Sorlie PD, Stein J, Towfighi A, Turan TN, Virani SS, Willey JZ, Woo D, Yeh RW, Turner MB. American Heart Association Statistics Committee and Stroke Statistics Subcommittee. Heart disease and stroke statistics – 2015 update: A report from the American Heart Association. Circulation. 2015; 131:e29–322. DOI: 10.1161/CIR.0000000000000152 [PubMed: 25520374]

Nandlall SD, Goldklang MP, Kalashian A, Dangra NA, D'Armiento JM, Konofagou EE. Monitoring and staging abdominal aortic aneurysm disease with pulse wave imaging. Ultrasound Med Biol. 2014; 40:2404–2414. DOI: 10.1016/j.ultrasmedbio.2014.04.013 [PubMed: 25130446]

Nieman BJ, Turnbull DH. Ultrasound and magnetic resonance microimaging of mouse development. Methods Enzymol. 2010; 476:379–400. DOI: 10.1016/S0076-6879(10)76021-3 [PubMed: 20691877]

Nieman BJ, Szulc KU, Turnbull DH. Three-dimensional in vivo MRI with self-gating and image coregistration in the mouse. Magn Reson Med. 2009; 61:1148–1157. DOI: 10.1002/mrm.21945 [PubMed: 19253389]

Nomura-Kitabayashi A, Phoon CKL, Kishigami S, Rosenthal J, Yamauchi Y, Abe K, Yamamura K, Samtani R, Lo CW, Mishina Y. Outflow tract cushions perform a critical valve-like function in the early embryonic heart requiring BMPRIA-mediated signaling in cardiac neural crest. Am J Physiol Heart Circ Physiol. 2009; 297:H1617–H1628. DOI: 10.1152/ajpheart.00304.2009 [PubMed: 19717734]

Norris FC, Wong MD, Greene NDE, Scambler PJ, Weaver T, Weninger WJ, Mohun TJ, Henkelman RM, Lythgoe MF. A coming of age: Advanced imaging technologies for characterising the developing mouse. Trends Genet. 2013; 29:700–711. DOI: 10.1016/j.tig.2013.08.004 [PubMed: 24035368]

Pachon RE, Scharf BA, Vatner DE, Vatner SF. Best anesthetics for assessing left ventricular systolic function by echocardiography in mice. Am J Physiol Heart Circ Physiol. 2015; 308:H1525–H1529. DOI: 10.1152/ajpheart.00890.2014 [PubMed: 25862835]

Parasoglou P, Berrios-Otero CA, Nieman BJ, Turnbull DH. High-resolution MRI of early-stage mouse embryos. NMR Biomed. 2013; 26:224–231. DOI: 10.1002/nbm.2843 [PubMed: 22915475]

Peng Y, Popvić ZB, Sopko N, Drinko J, Zhang Z, Thomas JD, Penn MS. Speckle tracking echocardiography in the assessment of mouse models of cardiac dysfunction. Am J Physiol Heart Circ Physiol. 2009; 297:H811–H820. DOI: 10.1152/ajpheart.00385.2009 [PubMed: 19561310]

Petiet AE, Kaufman MH, Goddeeris MM, Brandenburg J, Elmore SA, Johnson GA. High-resolution magnetic resonance histology of the embryonic and neonatal mouse: A 4D atlas and morphologic database. Proc Natl Acad Sci USA. 2008; 105:12331–12336. DOI: 10.1073/pnas.0805747105 [PubMed: 18713865]

Phoon CKL. Circulatory physiology in the developing embryo. Curr Opin Pediatr. 2001; 13:456–464. DOI: 10.1097/00008480-200110000-00013 [PubMed: 11801893]

Phoon CKL. Imaging tools for the developmental biologist: Ultrasound biomicroscopy of mouse embryonic development. Pediatr Res. 2006; 60:14–21. DOI: 10.1203/01.pdr.0000219441.28206.79 [PubMed: 16690959]

Phoon CKL, Turnbull DH. Ultrasound biomicroscopy-Doppler in mouse cardiovascular development. Physiol Genomics. 2003; 14:3–15. DOI: 10.1152/physiolgenomics.00008.2003 [PubMed: 12824473]

Phoon CKL, Aristizábal O, Turnbull DH. 40 MHz Doppler characterization of umbilical and dorsal aortic blood flow in the early mouse embryo. Ultrasound Med Biol. 2000; 26:1275–1283. DOI: 10.1016/S0301-5629(00)00278-7 [PubMed: 11120365]

Phoon CKL, Aristizábal O, Turnbull DH. Spatial velocity profile in mouse embryonic aorta and Doppler-derived volumetric flow: A preliminary model. Am J Physiol Heart Circ Physiol. 2002; 283:908–916. DOI: 10.1152/ajpheart.00869.2001

Phoon CK, Ji RP, Chowdhury PD. Transposition of the great arteries and double outlet right ventricle have related early developmental origins: Fundamental insights from in vivo imaging. Circulation. 2007; 116(Suppl):511.

Phoon CKL, Ji RP, Aristizábal O, Worrad DM, Zhou B, Baldwin HS, Turnbull DH. Embryonic heart failure in NFATc1−/− mice: Novel mechanistic insights from in utero ultrasound biomicroscopy. Circ Res. 2004; 95:92–99. DOI: 10.1161/01.RES.0000133681.99617.28 [PubMed: 15166096]

Phoon CKL, Acehan D, Schlame M, Stokes DL, Edelman-Novemsky I, Yu D, Xu Y, Viswanathan N, Ren M. Tafazzin knockdown in mice leads to a developmental cardiomyopathy with early diastolic dysfunction preceding myocardial noncompaction. JAHA: J Am Heart Assoc. 2012; 1:jah3-e000455. JAHA.111.000455. [PubMed: 23130124]

Poole KM, Tucker-Schwartz JM, Sit WW, Walsh AJ, Duvall CL, Skala MC. Quantitative optical imaging of vascular response in vivo in a model of peripheral arterial disease. Am J Physiol Heart Circ Physiol. 2013; 305:H1168–H1180. DOI: 10.1152/ajpheart.00362.2013 [PubMed: 23955718]

Prieto C, Andia ME, von Bary C, Onthank DC, Schaeffter T, Botnar RM. Accelerating three-dimensional molecular cardiovascular MR imaging using compressed sensing. J Magn Reson Imaging. 2012; 36:1362–1371. DOI: 10.1002/jmri.23763 [PubMed: 22865680]

Ram R, Mickelsen DM, Theodoropoulos C, Blaxall BC. New approaches in small animal echocardiography: Imaging the sounds of silence. Am J Physiol Heart Circ Physiol. 2011; 301:H1765–1780. DOI: 10.1152/ajpheart.00559.2011 [PubMed: 21873501]

Roth DM, Swaney JS, Dalton ND, Gilpin EA, Ross J Jr. Impact of anesthesia on cardiac function during echocardiography in mice. Am J Physiol Heart Circ Physiol. 2002; 282:H2134–H2140. DOI: 10.1152/ajpheart.00845.2001 [PubMed: 12003821]

Ruijter JM, Soufan AT, Hagoort J, Moorman AFM. Molecular imaging of the embryonic heart: Fables and facts on 3D imaging of gene expression patterns. Birth Defects Res Part, C. 2004; 72:224–240. DOI: 10.1002/bdrc.20018

Scherrer-Crosbie M, Kurtz B. Ventricular remodeling and function: Insights using murine echocardiography. J Mol Cell Cardiol. 2010; 48:512–517. DOI: 10.1016/j.yjmcc.2009.07.004 [PubMed: 19615377]

Schneider JE, Böse J, Bamforth SD, Gruber AD, Broadbent C, Clarke K, Neubauer S, Lengeling A, Bhattacharya S. Identification of cardiac malformations in mice lacking Ptdsr using a novel high-throughput magnetic resonance imaging technique. BMC Dev Biol. 2004; 4:16.doi: 10.1186/1471-213X-4-16 [PubMed: 15615595]

Sharpe J, Ahlgren U, Perry P, Hill B, Ross A, Hecksher-Serensen J, Baldock R, Davidson D. Optical projection tomography as a tool for 3D microscopy and gene expression studies. Science. 2002; 296:541–545. DOI: 10.1126/science.1068206 [PubMed: 11964482]

Smith BR. Magnetic resonance imaging analysis of embryos. Methods Mol Biol. 2000; 135:211–216. [PubMed: 10791318]

Smith BR. Magnetic resonance microscopy in cardiac development. Microsc Res Tech. 2001; 52:323–330. DOI: 10.1002/1097-0029(20010201)52:3<3c323::AID-JEMT1016>3e3.0.CO;2-F [PubMed: 11180623]

Smith BR, Johnson GA, Groman EV, Linney E. Magnetic resonance microscopy of mouse embryos. Proc Natl Acad Sci USA. 1994; 91:3530–3533. DOI: 10.1073/pnas.91.9.3530 [PubMed: 8170941]

Srinivasan S, Baldwin HS, Aristizabal O, Kwee L, Labow M, Artman M, Turnbull DH. Noninvasive, in utero imaging of mouse embryonic heart development with 40-MHz echocardiography. Circulation. 1998; 98:912–918. DOI: 10.1161/01.CIR.98.9.912 [PubMed: 9738647]

Thibault HB, Kurtz B, Raher MJ, Shaik RS, Waxman A, Derumeaux G, Halpern EF, Bloch KD, Scherrer-Crosbie M. Noninvasive assessment of murine pulmonary arterial pressure: Validation and application to models of pulmonary hypertension. Circ Cardiovasc Imaging. 2010; 3:157–163. DOI: 10.1161/CIRCIMAGING.109.887109 [PubMed: 20044514]

Turnbull DH, Mori S. MRI in mouse developmental biology. NMR Biomed. 2007; 20:265–274. DOI: 10.1002/nbm.1146 [PubMed: 17451170]

Vandsburger MH, Epstein FH. Emerging MRI methods in translational cardiovascular research. J Cardiovasc Transl Res. 2011; 4:477–492. DOI: 10.1007/s12265-011-9275-1 [PubMed: 21452060]

Vinegoni C, Fumene Feruglio P, Razansky D, Gorbatov R, Ntziachristos V, Sbarbati A, Nahrendorf M, Weissleder R. Mapping molecular agents distributions in whole mice hearts using born-normalized optical projection tomography. PLoS One. 2012; 7:e34427.doi: 10.1371/journal.pone.0034427 [PubMed: 22509302]

Wadghiri YZ, Schneider AE, Gray EN, Aristizabal O, Berrios C, Turnbull DH, Gutstein DE. Contrast-enhanced MRI of right ventricular abnormalities in Cx43 mutant mouse embryos. NMR Biomed. 2007; 20:366–374. DOI: 10.1002/nbm.1113 [PubMed: 17451172]

Walls JR, Coultas L, Rossant J, Henkelman RM. Three-dimensional analysis of vascular development in the mouse embryo. PLoS One. 2008; 3:e2853.doi: 10.1371/journal.pone.0002853 [PubMed: 18682734]

Wang X, Hagemeyer CE, Hohmann JD, Leitner E, Armstrong PC, Jia F, Olschewski M, Needles A, Peter K, Ahrens I. Novel single-chain antibody-targeted microbubbles for molecular ultrasound imaging of thrombosis: Validation of a unique noninvasive method for rapid and sensitive detection of thrombi and monitoring of success or failure of thrombolysis in mice. Circulation. 2012; 125:3117–3126. DOI: 10.1161/CIRCULATIONAHA.111.030312 [PubMed: 22647975]

Yang J, Yu LX, Rennie MY, Sled JG, Henkelman RM. Comparative structural and hemodynamic analysis of vascular trees. Am J Physiol Heart Circ Physiol. 2010; 298:H1249–59. DOI: 10.1152/ajpheart.00363.2009 [PubMed: 20081111]

Zamyadi M, Baghdadi L, Lerch JP, Bhattacharya S, Schneider JE, Henkelman RM, Sled JG. Mouse embryonic phenotyping by morphometric analysis of MR images. Physiol Genomics. 2010; 42A:89–95. DOI: 10.1152/physiolgenomics.00091.2010 [PubMed: 20682847]

Zhang X, Schneider JE, Portnoy S, Bhattacharya S, Henkelman RM. Comparative SNR for high-throughput mouse embryo MR microscopy. Magn Reson Med. 2010; 63:1703–1707. DOI: 10.1002/mrm.22352 [PubMed: 20512875]

Zhang X, Ha S, Wei W, Duan S, Shi Y, Yang Y. Noninvasive imaging of aortic atherosclerosis by ultrasound biomicroscopy in a mouse model. J Ultrasound Med. 2015; 34:111–116. DOI: 10.7863/ultra.34.1.111 [PubMed: 25542946]

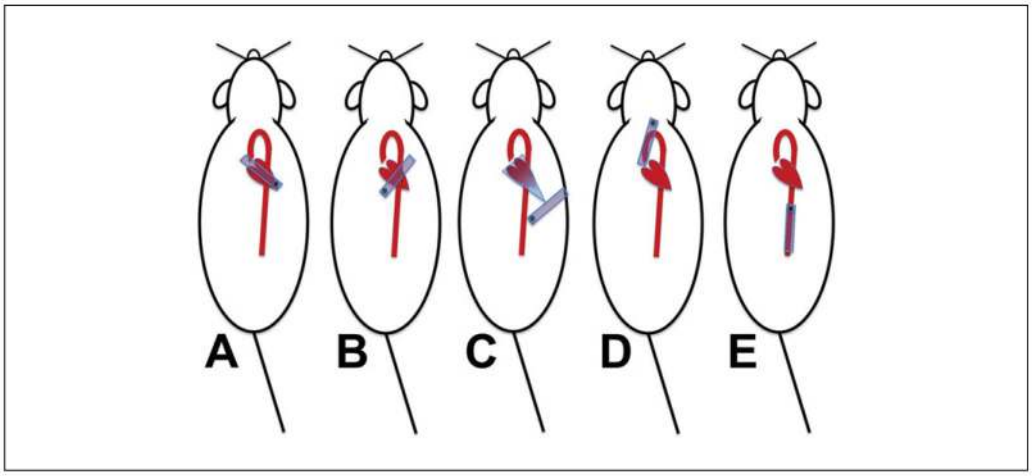

Figure 1.

Transducer placement and echocardiographic imaging planes. (**A**) Parasternal long axis view. The transducer (blue rectangle) is oriented along the long axis of the heart, typically with the long edge of the probe aimed towards the right shoulder of the mouse. The imager must move up or down the chest to obtain an appropriately angled image (see Fig. 2). (**B**) Parasternal short axis view. If the heart is orthogonal to the transducer, all that needs to be done is to rotate the transducer 90° clockwise. The mid-LV level is good for determination of cardiac function (level of the mitral valve papillary muscles); while at the base of the heart, the aortic valve and pulmonary arteries can be seen. (**C**) Apical 4-chamber view. A true apical view that displays all four chambers cannot be obtained most of the time in the mouse, but one can usually obtain a foreshortened left ventricle with mitral inflow and aortic outflow. (**D**) Aortic arch view. The transducer must be positioned high into the neck, slightly off-vertical as shown, and aimed slightly downward. The imager must be careful not to exert any pressure since this will often lead to profound bradycardia and possible airway compression. (**E**) Abdominal aorta. The transducer is placed just below the xiphoid process, and the abdominal aorta may be imaged in either the longitudinal plane (as shown) or the cross-sectional plane (rotate the transducer 90°).

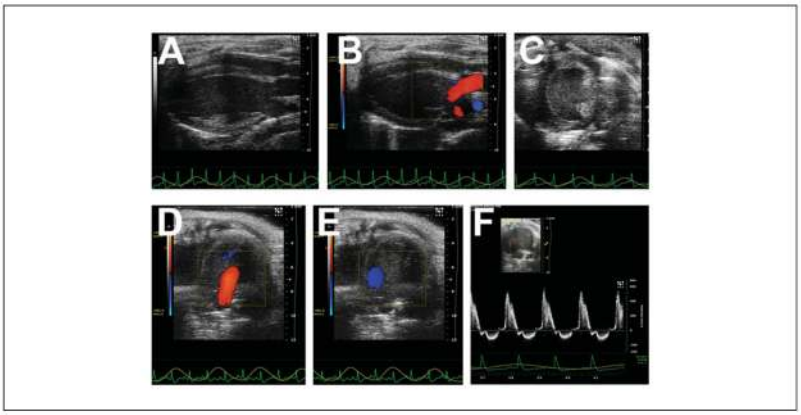

Figure 2.

Heart images from different planes. (**A**) Parasternal long axis view. The left ventricular apex is to our left, with the mitral valve, aortic valve, and aortic root shown. Note how the heart lies "flat" and is orthogonal to the transducer, and the normal left ventricle is shaped like a prolate ellipsoid ("bullet shaped"). (**B**) Parasternal long axis view, with superimposed color Doppler flow map, showing mitral inflow and aortic outflow. (**C**) Parasternal short axis view. The normal left ventricle is round, and systolic function is normally determined at the level of the papillary muscles. The right ventricle is often poorly seen. (**D**) Apical 4-chamber view, with superimposed color Doppler flow map showing mitral inflow (red jet). (**E**) Apical 4-chamber view, with superimposed color Doppler flow map showing aortic outflow (blue jet). (**F**) Pulsed-wave Doppler signal of mitral inflow plus off-angle aortic outflow.

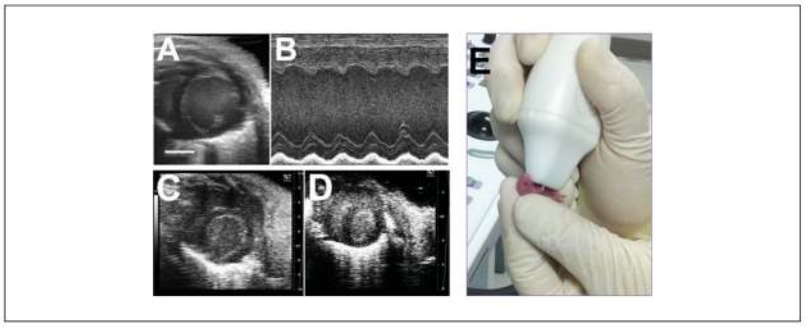

Figure 3.

Parasternal short axis imaging of the left ventricle through the ages. (**A**) Adult heart. (**B**) Corresponding M-mode echocardiogram. (**C**) Juvenile (few weeks old, post-weaning). (**D**) Newborn pup. Note the far grainier image. (**E**) Newborn pup being imaged. The pup is held very gently with the thumb and forefinger, and ultrasound gel is applied all over the chest, taking care not to cover the snout. Parasternal long and short axis imaging can be accomplished in this manner. Scale bars (A, C, D): 2 mm.

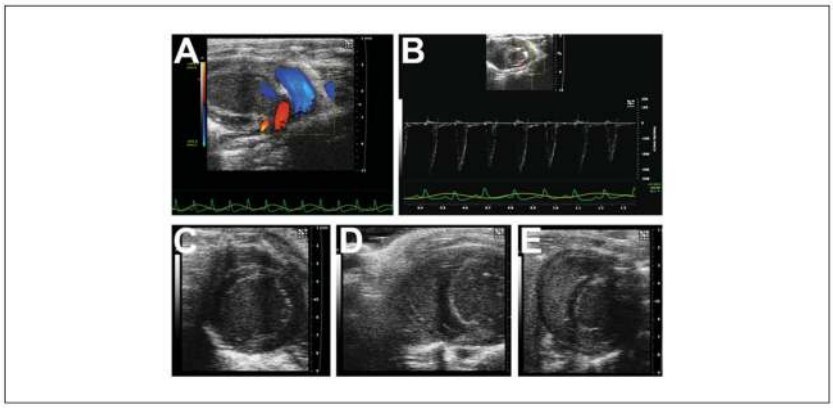

Figure 4.

Pulmonary and right ventricular imaging. (**A**) From the parasternal long axis view, tilting the transducer leftwards will open up the pulmonary artery, and this image shows a superimposed color Doppler map showing normal pulmonary arterial flow (blue jet). (**B**) Pulsed-wave Doppler signal in the main pulmonary artery. (**C**) Typical parasternal short axis imaging of the left ventricle will not yield good images of the right ventricle, but sliding the transducer towards the right parasternal edge may yield limited images of the right ventricle (**D**,**E**).

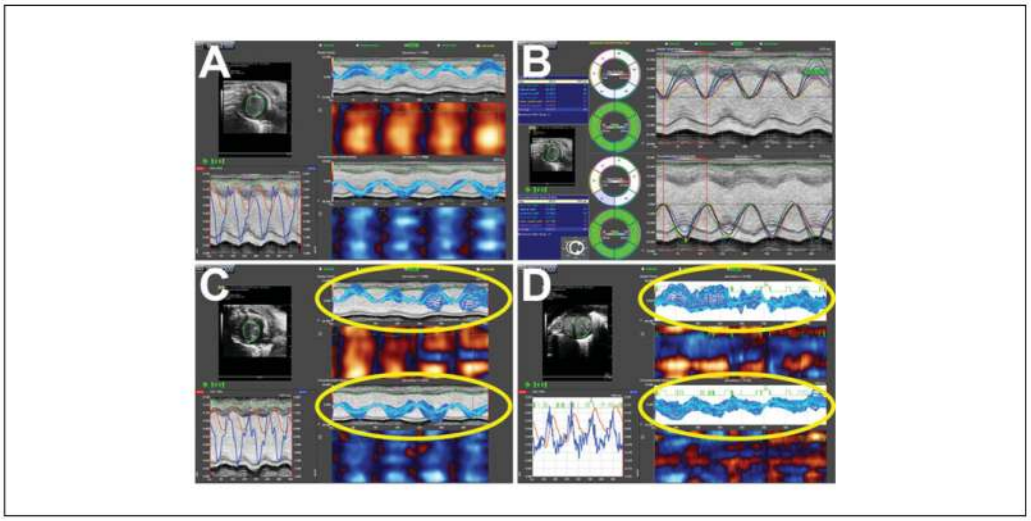

Figure 5.

Strain imaging on the Vevo 2100 system. (**A**) Normal heart, with nearly ideal data. (**B**) Time-to-peak analysis. (**C** and **D**) Examples of poor strain data and pitfalls of strain imaging (highlighted areas). In C, the speckle tracking is poor, even though the heart is normal, resulting in wide variations in strain during systole. D shows our typical experience with newborn pup hearts, which do not appear to track well at all, despite reasonable B-mode images.

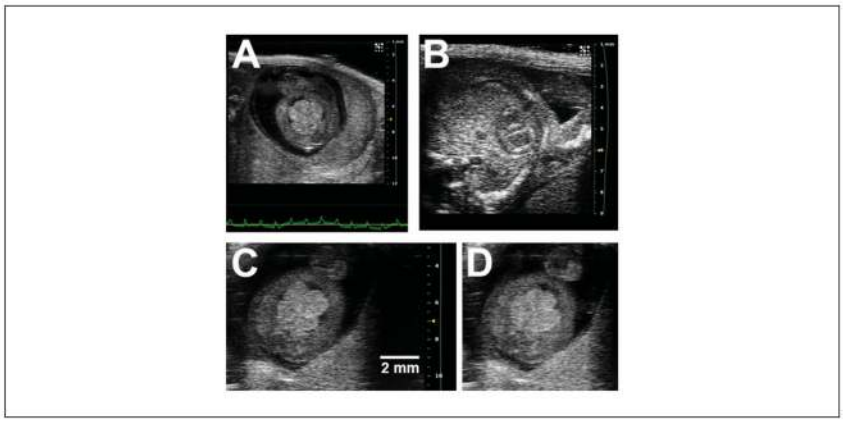

Figure 6.

Noninvasive (transabdominal) embryonic/fetal heart imaging. (**A**) 4-chamber view of the E13.5 embryonic heart. Note how the intraluminal blood is echogenic. (**B**) Short axis view of the fetal E18.5 ventricles. Note how the intraluminal blood at this later stage is now relatively echolucent. (**C** and **D**) Method for measuring systolic ventricular function. The combined left and right ventricular areas are traced at end-diastole (C) and end-systole (D) to yield the fractional area shortening.

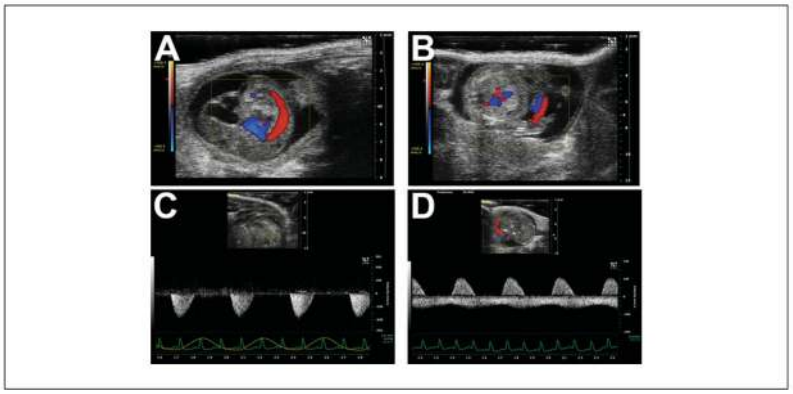

Figure 7.

Examples of arterial flow in the prenatal mouse. (**A**) Sagittal view of an E12.5 mouse embryo, with superimposed color Doppler flow map showing the dorsal aorta. (**B**) Color Doppler flow map of the umbilical vessels (red-blue "stripes" to the right of center; placenta is the homogeneous gray region below the embryo). (**C**) Pulsed-wave Doppler signal in the dorsal aorta (not the same embryo as in A). (**D**) Pulsed-wave Doppler signal in the umbilical cord (not the same embryo as in B). The pulsatile positive deflection is the umbilical artery, while the more continuous negative deflection is the umbilical vein. In C and D, the maternal EKG and respiratory waveforms are shown at the bottom, which help monitor the pregnant mouse during embryonic/fetal imaging.

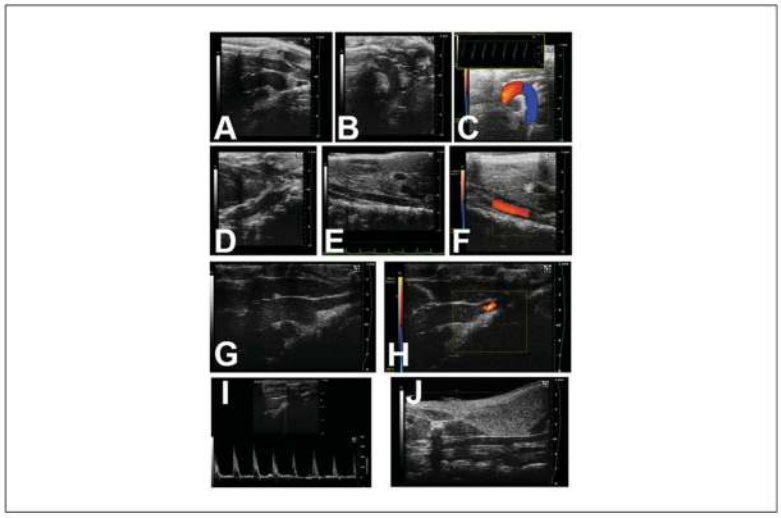

Figure 8.

Imaging of the aorta (may require multiple imaging planes) and its branches. (**A**) Ascending aorta and very proximal aortic arch. (**B**) Aortic arch and very proximal thoracic descending aorta. (**C**) Color Doppler flow map of aortic arch (inset: pulsed-wave Doppler signal of the distal aortic arch). (**D**) Thoracic descending aorta, behind the heart. (**E**) Abdominal aorta, near the level of the kidneys. (**F**) Abdominal aorta with superimposed color Doppler flow map. The brachiocephalic branches off the aortic arch may also be imaged. (**G**) Distal ascending aorta, with innominate artery takeoff. (**H**) Same as (G), but the superimposed color Doppler flow map showing normal flow into the innominate artery. (**I**) Pulsed-wave Doppler signal of the proximal innominate artery. (**J**) Right common carotid artery, further up into the neck.

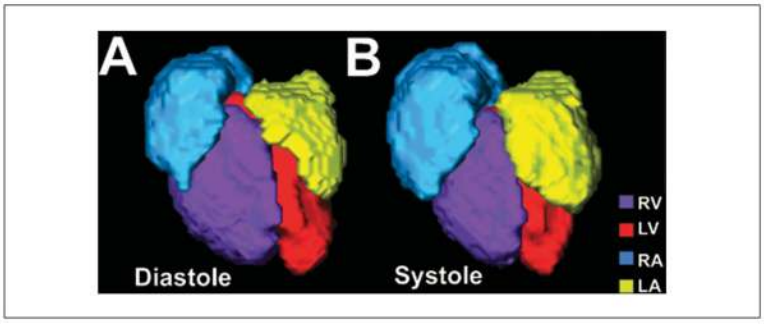

Figure 9.

In utero MRI of an E17.5 fetal mouse heart. After motion correction and cardiac gating, color coded volumetric renderings of the four chambers in a beating fetal mouse heart shows differences between diastole (**A**) and systole (**B**). Right ventricle, RV (purple); left ventricle, LV (red); right atrium, RA (blue); left atrium, LA (yellow).

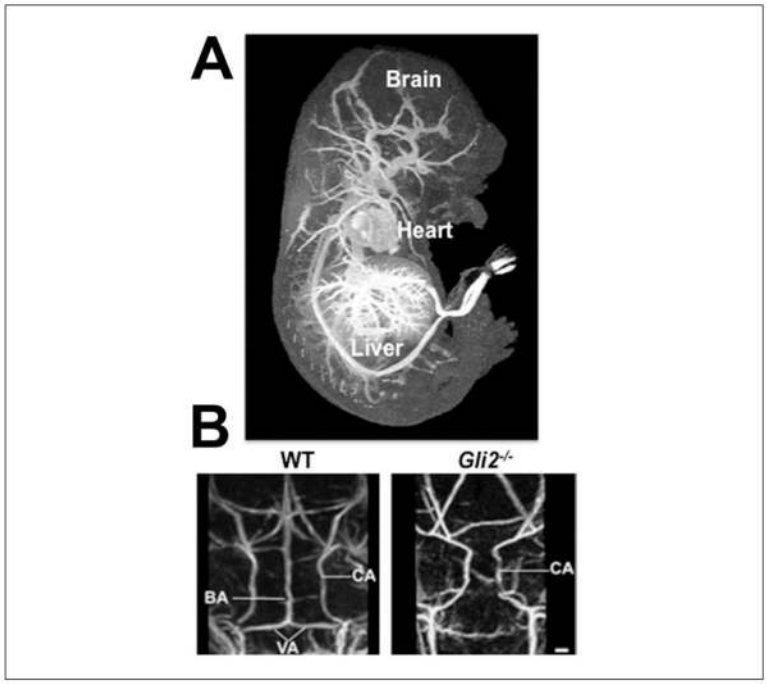

Figure 10.

Ex vivo MRI of perfusion-fixed, gadolinium (Gd)-enhanced E17.5 mouse embryonic vasculature. (**A**) Following perfusion-fixation with the BSA-DTPA-Gd-gelatin solution, a maximum intensity projection (MIP) through the 3D, T1-weighted MRI data set, viewed from the side, shows the heart and vasculature in the brain, liver, and other regions of the embryo. (**B**) MIPs of wild-type (WT; left) and *Gli2*$^{-/-}$ mutant (right) embryos, viewed from the back, show the missing basilar artery (BA) in the mutant, a vascular phenotype that was discovered using MRI. Other vessels labeled are the carotid (CA) and vertebral (VA) arteries.

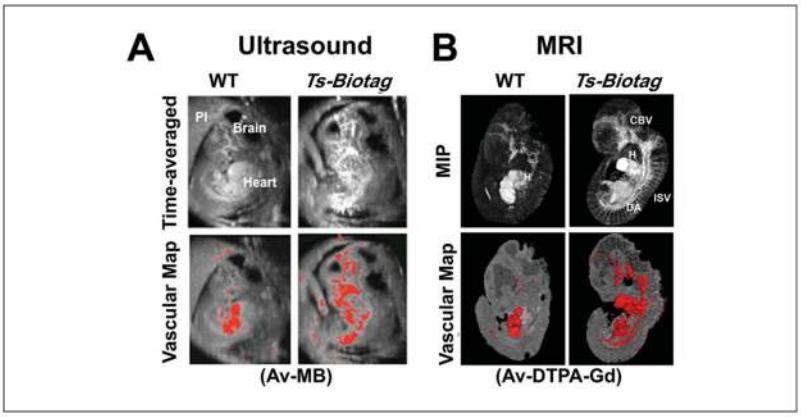

Figure 11.

Molecular imaging of E11.5 mouse embryonic vasculature. The Biotag transgene was expressed from the *Tie2* promoter-enhancer elements in *Ts-Biotag* vascular reporter mice. (**A**) Time-averaged cine ultrasound biomicroscopy images were acquired 20 min after intravascular injection of avidinated microbubbles (Av-MB). Av-MB binding and enhancement in *Ts-Biotag* embryos compared to wild-type (WT) littermates allowed visualization of embryonic vasculature and quantitation of vascular maps after threshold segmentation (bottom panels). (**B**) Similar experiments using MRI after injection of avidin-conjugated to DTPA-Gd (Av-DTPA-Gd) showed vascular labeling in maximum intensity projection (MIP) images and quantitative vascular maps. Cerebral blood vessels, CBV; dorsal aorta, DA; heart, H; intersomitic vessels, ISV; placenta, Pl.

Table 1

Selected Echocardiographic Measurements[a]

Echocardiographic modality	Measurements
B-mode	LV end-diastolic dimension
	LV end-systolic dimension
	LV wall thickness (septal)
	LV wall thickness (posterior wall)
	Shortening fraction
	Ejection fraction
	Fractional area shortening
	LV mass
	Vessel diameters
	Intima-media thickness
Spectral Doppler	Heart rate
	Isovolumic contraction time
	Isovolumic relaxation time
	Ejection time (LV, RV)
	Myocardial performance (Tei) index (MPI)
	Velocity-time integral
	E and A waves (trans-mitral flow)
	Peak flow velocity (aortic, pulmonary, umbilical artery/vein, other)
Color Doppler flow mapping	Atrioventricular valve regurgitation
	Outflow tract (aortic, pulmonary) valve regurgitation
	Valvular stenosis, obstruction
	Transverse aortic constriction
Derived parameters (combination of other measurements)	Stroke volume
	Cardia output
	Coronary flow reserves
Strain and strain rate	Peak segmental strain
	Peak segmental strain rate
	Peak global strain
	Peak global strain rate
	Time to peak strain

[a]Phoon et al., 2000; Phoon et al., 2002; Phoon and Turnbull, 2003; Liu and Rigel, 2009; Gao et al., 2011; Ram et al., 2011; Fayssoil et al., 2013; Moran et al., 2013.